Wave-packet continuum-discretization approach to single ionization of helium by antiprotons and energetic protons

I. B. Abdurakhmanov, A. S. Kadyrov, and I. Bray
Curtin Institute for Computation and Department of Physics, Astronomy and Medical Radiation Science, Curtin University, GPO Box U1987, Perth, WA 6845, Australia

K. Bartschat
Department of Physics and Astronomy, Drake University, Des Moines, Iowa 50311, USA
(Received 13 July 2017; published 4 August 2017)

The recently developed wave-packet continuum-discretization approach [I. B. Abdurakhmanov, A. S. Kadyrov, and I. Bray, Phys. Rev. A **94**, 022703 (2016)] is extended to antiproton-helium collisions. The helium target is treated as a three-body Coulomb system using a frozen-core approximation, in which the electron-electron correlation within the target is accounted for through the static interaction. The Schrödinger equation for the helium target is solved numerically to yield bound and continuum states of the active electron. The resulting continuum state is used to construct wave-packet pseudostates with arbitrary energies. The energies of the pseudostates are chosen in a way that is ideal for detailed differential ionization studies. Two-electron target wave functions, formed from the bound and continuum wave-packet states of the active electron and the 1s orbital of He^+, are then utilized in the single-center semiclassical impact-parameter close-coupling scheme. A comprehensive set of benchmark results, from angle-integrated to fully differential cross sections for antiproton impact single ionization of helium in the energy range from 1 keV to 1 MeV, is provided. Furthermore, we use our single-center convergent close-coupling approach to study fully differential single ionization of helium by 1-MeV proton impact. The calculated results are in good agreement with recent experimental measurements [H. Gassert, O. Chuluunbaatar, M. Waitz, F. Trinter, H.-K. Kim, T. Bauer, A. Laucke, C. Müller, J. Voigtsberger, M. Weller *et al.*, Phys. Rev. Lett. **116**, 073201 (2016)] for all considered geometries.

DOI: 10.1103/PhysRevA.96.022702

I. INTRODUCTION

Studies of processes taking place in ion-atom collisions are not only of fundamental interest but they have numerous practical applications, including nuclear fusion reactors, hadron therapy, transport of ions through gaseous and solid targets, atmospheric science, astrophysics, etc. [1,2]. From a theoretical point of view, accurate and reliable modeling of the relevant processes over a wide range of projectile energies requires the development of sophisticated computational approaches. The prototype of ion-atom collisions, which served as a starting point for many theoretical approaches [3–11], is the collision of antiprotons with atomic hydrogen. In the regions of practical interest, this process can safely be considered without accounting for rearrangement channels that lead to protonium formation.

Recently, we developed a close-coupling approach to this collision system based on wave-packet continuum discretization [12]. When compared to other close-coupling models, a distinct feature of our approach is its ability to generate the target continuum pseudostates with arbitrary ejection energies. In principle, these can be aligned across different angular momenta of the target electron, which greatly improves the accuracy of differential ionization studies. The above approach, therefore, is ideal for calculating the most detailed fully differential cross sections (FDCSs).

The idea of a wave-packet-based continuum-discretization approach to the target description can be extended to more complex targets. Regarding the level of computational complexity, the next target to consider is helium, i.e., a two-electron system. Antiproton-helium scattering is, in fact, the simplest quantum-mechanical four-body problem that allows for studying electron-correlation effects of the target.

The currently available theoretical approaches applied to this system mainly differ in two aspects: (i) the way the corresponding four-body Schrödinger equation (SE) is solved and (ii) the treatment of the helium target. Earlier works [13,14] based on perturbative methods produced reasonable results for several integrated cross sections representing single-electron processes at high impact energies. More sophisticated approaches [4,5,15–24] are based on the semiclassical close-coupling formalism, in which the antiproton motion is treated classically by means of straight-line trajectories. This approximation is well accepted in ion-atom collisions. Its validity to reproduce reliable integrated cross sections for all processes involved in antiproton-helium collisions above 1 keV was demonstrated in Refs. [25,26], where comparisons were made with predictions from fully quantum-mechanical treatments of the problem.

Various approaches were developed to address the electron-correlation effects in the target. Close-coupling calculations [4,5,15,18,19,24] that do not solve the SE directly, but rather convert it into a set of coupled differential equations by expanding the total scattering wave function in terms of target pseudostates, can only produce cross sections for single-ionization processes. Within the framework of such a close-coupling scheme, a number of works assumed a static correlation of the outer electron with the inner one confined to the 1s orbital, i.e., the frozen-core (FC) approximation. More sophisticated calculations by Igarashi *et al.* [15], Pindzola *et al.* [21], and Foster *et al.* [22], which allowed for multiple configurations for

both target electrons, produced total ionization cross sections that differed considerably from the values obtained in the frozen-core approximation. However, in these calculations the type of basis functions used to diagonalize the target Hamiltonian does not allow for inclusion of double-continuum states in the description of the He structure, since one would run into the problem of mixing single- and double-ionization channels. The root of the problem lies in the fact that for different configurations of the target electrons the energy levels of the individual one-electron functions that construct the helium states are generated randomly and not aligned. A combination of multiple electronic configurations of the target, represented by the product of one-electron functions with different continuum energy distributions, produce target state wave functions that do not allow for separating one-electron processes from the processes where both electrons are involved.

Borbély *et al.* [27] reported accurate total and doubly differential cross sections obtained by directly solving the fully correlated two-electron time-dependent Schrödinger equation using the time-dependent close-coupling method. Baxter and Kirchner [28,29] used time-dependent density-functional theory to investigate the role of electron correlations in the integrated single and double ionization in antiproton-helium collisions.

Technically, the problem can be addressed effectively with the use of wave packets. Helium wave packets can be obtained in several steps. First, following the configuration-interaction approach, the helium wave function is expressed as a linear combination of products of two one-electron functions. Next, a basis of N_1 He^+ radial functions representing the bound and continuum eigenstates of one of the electrons is created. This step can be carried out fully analytically. In the third step, the two-electron helium wave function, which contains the He^+ radial functions calculated in the previous step, is inserted into the appropriate SE for the helium target. This converts the target SE into a set of coupled integrodifferential equations for N_2 radial functions representing the state of the second electron. This set of integrodifferential equations is solved numerically subject to appropriate asymptotic boundary conditions.

As a result, a set of $N_1 \times N_2$ one-electron functions representing various electronic configurations is obtained. Some of the one-electron radial functions from this set represent continuum states of the electrons. These states are not normalizable and, consequently, are not suited for close-coupling scattering calculations. However, this issue can be resolved using the technique that was applied to the description of atomic hydrogen [12], namely, one-electron radial functions representing continuum states are replaced by normalizable wave packets. Each of these wave packets represents nonoverlapping subregions of the continuum and are the integrals of continuum functions over the corresponding subregion. In constructing wave packets for each electronic configuration, it is necessary to use the same grid when discretizing the continuum. This avoids any mixture of various single- and double-ionization and excitation channels.

The wave-packet-based model of the helium target described in this paper not only benefits the current status of theoretical studies of collisions involving helium targets but it will also serve as the background for developing a powerful approach to collisions with diatomic molecules. Such an approach will allow for conducting currently unavailable differential ionization studies of molecular targets.

The idea of a wave-packet-based description of the target was previously applied to ionization of helium by Barna *et al.* [30]. The authors constructed a basis of He one-electron functions from Slater orbitals and wave packets built from hydrogenic Coulomb functions. Reasonable results for single- and double-ionization cross sections were obtained at high impact energies.

As a starting point for the present paper, we will develop a semiclassical one-center close-coupling approach to antiproton-helium scattering based on a wave-packet continuum-discretization procedure, with one of the helium electrons being confined to the 1*s* orbital. As described above, the continuous spectrum of the second electron is discretized using the wave packets constructed from the continuum wave function, using the eigenstates of the frozen-core target Hamiltonian. The approach starts from the semiclassical four-body SE for the scattering wave function and leads to a set of coupled differential equations for the transition probability amplitudes. To demonstrate the utility of the method, various cross sections, from angle-integrated to fully differential, will be calculated for single-electron processes occurring in antiproton-helium collisions.

Comparison of the prediction with experimental data from recent measurements of fully differential single-ionization cross sections for the scattering of energetic 1-MeV protons on helium targets [31] will also be used to test the developed approach comprehensively. The experimental setup, based on the well-established cold-target recoil-ion momentum spectroscopy technique, allowed for obtaining the highest resolution in the ejected-electron angular distribution data ever reported in the collision plane, as well as generating data in several other planes. Generally good agreement was reported [31] between the measured data and first Born calculations for all planar geometries considered.

This was not the case for the differential studies of single ionization of helium under the impact of heavier projectiles of C^{6+}. The experiment for C^{6+} projectiles [32] initiated numerous discussions in the field. Even today, the most advanced theories remain in strong disagreement with the measurements of the fully differential single-ionization cross sections for the plane perpendicular to the momentum transfer direction. The question whether this disagreement is due to shortages in the theoretical approaches or insufficient experimental resolution still needs to be answered. In this regard it is interesting to see whether more sophisticated close-coupling calculations of proton impact single ionization of helium might yield significant corrections to the first Born calculations, especially for the perpendicular plane geometry.

The single-center close-coupling approach developed in the present paper is capable of producing cross sections to compare with the measured differential ionization data. At the experimentally considered collision energy of 1 MeV, the electron capture channels are several orders of magnitude less important than the direct ionization channel. In this regime, therefore, single-center approaches are expected to be reliable for studying also the scattering of positively charged projectiles.

In Sec. II we give a brief outline of the formalism and describe the procedure for generating the wave packets. Details of the calculations are described in Sec. III, and the results are presented in Sec. IV. Finally, in Sec. V, we highlight the principal findings and draw conclusions from the present paper. Unless specified otherwise, atomic units are used throughout this paper.

II. WAVE-PACKET APPROACH

We treat antiproton-helium scattering within the framework of the one-center semiclassical convergent close-coupling (CCC) method developed previously [12,33,34]. The approach follows from the exact four-body formalism, where the total scattering wave function Ψ_i^+ satisfies the nonrelativistic Schrödinger equation

$$(H - E)\Psi_i^+ = 0. \tag{1}$$

The four-body Hamiltonian operator H is written as

$$H = -\frac{\nabla_{\boldsymbol{R}}^2}{2\mu} - \frac{\nabla_{\boldsymbol{r}_1}^2}{2} - \frac{\nabla_{\boldsymbol{r}_2}^2}{2} - \frac{2}{r_1} - \frac{2}{r_2} + \frac{1}{|\boldsymbol{R} - \boldsymbol{r}_1|} + \frac{1}{|\boldsymbol{R} - \boldsymbol{r}_2|} - \frac{2}{R}, \tag{2}$$

where μ is the reduced mass of the projectile-target system, while $\boldsymbol{R}$, $\boldsymbol{r}_1$, and $\boldsymbol{r}_2$ are the positions of the incident antiproton and the two orbital electrons relative to the helium nucleus. The target nucleus is located at the origin, and we assume that the projectile is moving along a classical trajectory $\boldsymbol{R} \equiv \boldsymbol{R}(t) = \boldsymbol{b} + \boldsymbol{v}t$, where $\boldsymbol{b}$ is the impact parameter and $\boldsymbol{v}$ is the initial velocity of the projectile relative to the target. It is defined such that $\boldsymbol{b} \cdot \boldsymbol{v} = 0$.

We separate the total scattering wave function Ψ_i^+ into nuclear and electronic parts according to (see, e.g., Bransden and McDowell [35])

$$\Psi_i^+ = e^{i\boldsymbol{q}\cdot\boldsymbol{R}}\Psi_{\rm e}, \tag{3}$$

where $\boldsymbol{q}$ is the incident momentum of the projectile relative to the target nucleus. After inserting this into Eq. (1) and using the semiclassical approximation, we obtain the nonrelativistic semiclassical time-dependent Schrödinger equation for the electronic part of the total scattering wave function:

$$(H_{\rm t} + V)\Psi_{\rm e}(t,\boldsymbol{r}_1,\boldsymbol{r}_2,\boldsymbol{R}) = i\frac{\partial\Psi_{\rm e}(t,\boldsymbol{r}_1,\boldsymbol{r}_2,\boldsymbol{R})}{\partial t}. \tag{4}$$

Here $H_{\rm t}$ is the target Hamiltonian

$$H_{\rm t} = -\frac{\nabla_{\boldsymbol{r}_1}^2}{2} - \frac{\nabla_{\boldsymbol{r}_2}^2}{2} - \frac{2}{r_1} - \frac{2}{r_2} + \frac{1}{|\boldsymbol{r}_1 - \boldsymbol{r}_2|}, \tag{5}$$

and

$$V = -\frac{2}{R} + \frac{1}{|\boldsymbol{R} - \boldsymbol{r}_1|} + \frac{1}{|\boldsymbol{R} - \boldsymbol{r}_2|} \tag{6}$$

is the interaction potential between the projectile and the target constituents.

The scattering wave function is expanded in terms of basis functions $\psi_\alpha(\boldsymbol{r}_1,\boldsymbol{r}_2)$, which are suitably chosen to represent the entire set of target states, as

$$\Psi_{\rm e}(t,\boldsymbol{r}_1,\boldsymbol{r}_2,\boldsymbol{R}) = \sum_{\alpha=1}^{N} a_\alpha(t,\boldsymbol{b})\psi_\alpha(\boldsymbol{r}_1,\boldsymbol{r}_2)e^{-i\epsilon_\alpha t}, \tag{7}$$

where N is the number of basis functions and ϵ_α is the energy of the target electronic state α. The latter collectively denotes the full set of quantum numbers representing that state. The expansion coefficients $a_\alpha(t,\boldsymbol{b})$ at $t \to +\infty$ represent the transition amplitudes into the various target states.

Substituting this representation of the scattering wave function into the semiclassical Schrödinger equation (4), and using the orthogonality properties of the basis functions, one obtains the following set of first-order differential equations for the time-dependent coefficients:

$$i\frac{da_\alpha(t,\boldsymbol{b})}{dt} = \sum_{\beta=1}^{N} e^{i(\epsilon_\alpha - \epsilon_\beta)t}\langle\psi_\alpha|V|\psi_\beta\rangle a_\beta(t,\boldsymbol{b}), \tag{8}$$

where $\alpha = 1,2,\ldots,N$. This system is solved subject to the initial boundary conditions

$$a_\alpha(-\infty,\boldsymbol{b}) = \delta_{\alpha,1s}, \tag{9}$$

which assume the atom is initially in the $1s$ state. If the basis functions are known, the matrix elements $\langle\psi_\alpha|V|\psi_\beta\rangle$ can be evaluated numerically [25].

A. Target description

In the quantum-mechanical convergent close-coupling (QM-CCC) approach [36], the two-electron helium target was described using the configuration interaction approach, where the target states were taken as a sum of products of one-electron orbitals. The one-electron orbitals were composed of orthogonal Laguerre functions. Two different approximations, frozen-core and multicore models of the helium target, were employed. In the frozen-core approximation, one of the electrons was confined to the $1s$ orbital. In addition to the bound states, the model also generated a set of positive-energy pseudostates that simulate the contribution of the entire continuum. Similar to the case of atomic hydrogen [12] the energies of the He continuum pseudostates for different values of the angular momentum l are not aligned, and there exist some difficulties with creating the desired energy distribution of the continuum pseudostates. Below we will extend the ideas of the wave-packet continuum-discretization approach to the two-electron helium target, which will allow us to construct basis states with arbitrary energies and distribution.

As shown in Ref. [12], the wave-packet continuum pseudostates for atomic hydrogen can be obtained by energy integration of the hydrogen continuum functions. For both bound and continuum states of atomic hydrogen, the Schrödinger equation has an analytical solution. Consequently, it was significantly easier to implement the wave-packet continuum-discretization approach for this target. For the helium atom, on the other hand, the Schrödinger equation needs to be solved numerically. As a first step, we develop a wave-packet-based description of the helium atom in the frozen-core approximation. Within this approximation and assuming that the total electronic spin of He, $S = 0$, is conserved during the

collision, the spatial part of the target wave function is written as

$$\psi_\alpha(\boldsymbol{r}_1,\boldsymbol{r}_2) = \phi_{1s}^{\mathrm{He}^+}(\boldsymbol{r}_2)\varphi_\alpha(\boldsymbol{r}_1) + \phi_{1s}^{\mathrm{He}^+}(\boldsymbol{r}_1)\varphi_\alpha(\boldsymbol{r}_2). \tag{10}$$

Here we use a single set of quantum numbers, α, for the target state, since only one electron can be excited. The total wave function of He is antisymmetric due to the antisymmetric spin-wave function of the singlet spin state. Then the Schrödinger equation for He becomes

$$H_t\psi_\alpha(\boldsymbol{r}_1,\boldsymbol{r}_2) = \left(\varepsilon_\alpha + \varepsilon_{1s}^{\mathrm{He}^+}\right)\psi_\alpha(\boldsymbol{r}_1,\boldsymbol{r}_2), \tag{11}$$

where ε_α is the state energy of the active electron and $\varepsilon_{1s}^{\mathrm{He}^+}$ is the energy of the frozen electron, which corresponds to the ground-state energy of He^+, i.e., -2 a.u. Substituting Eq. (10) into Eq. (11) and projecting onto $\phi_{1s}^{\mathrm{He}^+}$, we obtain the following integrodifferential equation for φ_α:

$$\begin{aligned}&\left[\nabla_{\boldsymbol{r}_1}^2 - 2V_{\mathrm{H}}(r_1) + 2\varepsilon_\alpha\right]\varphi_\alpha(\boldsymbol{r}_1)\\ &+ 2\varepsilon_\alpha\langle\phi_{1s}^{\mathrm{He}^+}|\varphi_\alpha\rangle\phi_{1s}^{\mathrm{He}^+}(\boldsymbol{r}_1)\\ &+ \langle\phi_{1s}^{\mathrm{He}^+}|\left[\nabla_{\boldsymbol{r}_2}^2 + \frac{4}{r_2}\right]|\varphi_\alpha\rangle_{\boldsymbol{r}_1}\phi_{1s}^{\mathrm{He}^+}(\boldsymbol{r}_1)\\ &- 2\langle\phi_{1s}^{\mathrm{He}^+}|\frac{1}{|\boldsymbol{r}_1-\boldsymbol{r}_2|}|\varphi_\alpha\rangle_{\boldsymbol{r}_1}\phi_{1s}^{\mathrm{He}^+}(\boldsymbol{r}_1) = 0,\end{aligned} \tag{12}$$

where

$$V_{\mathrm{H}}(r_1) = -2/r_1 + \langle\phi_{1s}^{\mathrm{He}^+}|\frac{1}{|\boldsymbol{r}_1-\boldsymbol{r}_2|}|\phi_{1s}^{\mathrm{He}^+}\rangle_{\boldsymbol{r}_1} \tag{13}$$

is the Hartree potential for $e-\mathrm{He}^+$ scattering. For negative-energy states of the active electron, the radial and angular parts are separable according to

$$\varphi_\alpha(\boldsymbol{r}) = R_{nl}(r)Y_{lm}(\hat{r}). \tag{14}$$

For positive-energy states, as

$$\varphi_\alpha(\boldsymbol{r}) \equiv \varphi_\kappa(\boldsymbol{r}) = \sqrt{\frac{2}{\pi}}\sum_{lm} i^l \exp(-i\eta_l)R_{\kappa l}(r)Y_{lm}^*(\hat{\kappa})Y_{lm}(\hat{r}), \tag{15}$$

where n,l, and m are the principal, orbital, and magnetic quantum numbers of the state α, κ is the momentum of the continuum state and η_l is the continuum phase shift.

For both negative and positive energies, Eq. (12) reduces to the following one-dimensional integrodifferential equation for the radial function $R_\alpha(r)$:

$$\begin{aligned}&\frac{d^2R_\alpha(r)}{dr^2} - \left[\frac{l(l+1)}{r^2} - \frac{4}{r} + 2W_0\left[R_{1s}^{\mathrm{He}^+},R_{1s}^{\mathrm{He}^+}\right] - 2\varepsilon_\alpha\right]R_\alpha(r)\\ &= \left[\frac{2}{2l+1}W_l\left[R_{1s}^{\mathrm{He}^+},R_\alpha\right]\right.\\ &\quad\left. - 2\int_0^\infty R_{1s}^{\mathrm{He}^+}(t)W_0\left[R_{1s}^{\mathrm{He}^+},R_{1s}^{\mathrm{He}^+}\right]R_\alpha(t)dt\right]R_{1s}^{\mathrm{He}^+}(r),\end{aligned} \tag{16}$$

where $R_{1s}^{\mathrm{He}^+}(r) = 4\sqrt{2}\exp(-2r)r$ and

$$W_l[f,g] = \frac{1}{r^{l+1}}\int_0^r f(t)g(t)t^l dt + r^l\int_r^\infty \frac{f(t)g(t)}{t^{l+1}}dt. \tag{17}$$

TABLE I. Energies (eV) of selected bound states of the helium atom. The present results are compared with the energies of the frozen-core Laguerre pseudostates (LPS) [36] and the data derived from optical spectra by Moore [37].

State	Present	LPS [36]	Moore [37]
$1s$	−23.7416	−23.74139	−24.5862
$2s$	−3.9035	−3.90343	−3.97155
$3s$	−1.6483	−1.64828	−1.66705
$2p$	−3.3307	−3.33198	−3.36931
$3p$	−1.48847	−1.48950	−1.50035
$3d$	−1.51024	−1.51150	−1.51329

Equation (16) is solved by iteration. The zeroth-order approximation $R_\alpha^{(0)}(r)$ is obtained by setting the right-hand side of Eq. (16) to zero. Subsequent approximations are derived using the previous-order approximations. At each iteration the linear inhomogeneous second-order differential equation for $R_\alpha^{(i)}(r)$ is solved by the Numerov method. The iteration process is continued until an accuracy $|R_\alpha^{(i+1)}(r) - R_\alpha^{(i)}(r)| < 10^{-5}$ is achieved for each point in the r grid. For the bound states of the active electron ($\varepsilon_\alpha < 0$), we require $\lim_{r\to\infty} R_\alpha(r) = 0$. The bound states are found by utilizing a standard shooting method by requiring the continuity of $R_\alpha(r)$ and $dR_\alpha(r)/dr$ at r_0, where

$$\frac{l(l+1)}{r^2} - \frac{4}{r} + 2W_0\left[R_{1s}^{\mathrm{He}^+},R_{1s}^{\mathrm{He}^+}\right] = 0. \tag{18}$$

For the continuum states, $R_\alpha(r)$ is matched to the Coulomb function at large r, which is also used to derive the continuum phase shift η_l. In the final step, the active-electron wave functions are normalized to satisfy

$$\langle R_{\alpha'}|R_\alpha\rangle = \delta_{\alpha'\alpha} \tag{19}$$

for bound states ($\varepsilon_\alpha < 0$) and

$$\langle R_{\alpha'}|R_\alpha\rangle = \delta(\kappa_{\alpha'} - \kappa_\alpha) \tag{20}$$

for the continuum states ($\varepsilon_\alpha > 0$).

Table I lists the results for the ionization potential of the selected helium bound states obtained by applying the Numerov method described above. The present results are compared with the corresponding energy levels of the frozen-core Laguerre pseudostates constructed from a basis of size $20-l$ and falloff parameter $\lambda_l = 1$ for $l = 0$–2, respectively. Also given are the benchmark results of Moore [37] derived from an analysis of optical spectra. At least a three-digit agreement is observed between the present results and the energy levels of the frozen-core Laguerre pseudostates. The derivation of bound states with higher energies requires a longer radial range in the solution of Eq. (16). According to Ref. [36], better agreement with the results of Moore [37] was achieved when relaxing a frozen-core approximation.

Unlike bound states, which only exist at discrete levels of the target energy spectrum, continuum states can be generated by solving Eq. (16) for arbitrary electron ejection energies. This greatly simplifies calculations of differential ionization cross sections in the first Born approximation (FBA). However, the non-normalizable nature of the He continuum wave

function makes it inapplicable for close-coupling scattering models.

To overcome this problem while keeping the flexibility of generating a state for arbitrary continuum energies, we use the wave-packet continuum-discretization approach, which was recently applied to describe the structure of atomic hydrogen [12]. To construct normalizable wave packets, we first take the continuous spectrum of the active electron with some maximum value of energy $E_{\max}$ and then divide the entire interval $[0,E_{\max}]$ into N_c nonoverlapping intervals (discretization bins) $[\mathcal{E}_{i-1},\mathcal{E}_i]_{i=1}^{N_c}$ with $\mathcal{E}_0=0$ and $\mathcal{E}_{N_c}=E_{\max}$. To obtain converged cross sections, $E_{\max}$ and N_c must be sufficiently large. Every such energy bin corresponds to the interval $[\kappa_{i-1},\kappa_i]$ in momentum space, where $\kappa_i=\sqrt{2\mathcal{E}_i}$. The wave packet (WP) corresponding to each of the bins is built from the following integral of the continuum function [which is the solution of Eq. (16)]:

$$R_{il}^{\mathrm{WP}}(r)=\nu_{il}\int_{\kappa_{i-1}}^{\kappa_i}d\kappa\,R_{\kappa l}(r), \tag{21}$$

where ν_{il} is the normalization coefficient. Then the wave packet based on two-electron helium wave functions is written as

$$\begin{aligned}\psi_\alpha^{\mathrm{WP}}(\boldsymbol{r}_1,\boldsymbol{r}_2)=&\,\phi_{1s}^{\mathrm{He}^+}(\boldsymbol{r}_2)R_{n_\alpha l_\alpha}^{\mathrm{WP}}(r_1)Y_{l_\alpha m_\alpha}(\hat{\boldsymbol{r}}_1)\\&+\phi_{1s}^{\mathrm{He}^+}(\boldsymbol{r}_1)R_{n_\alpha l_\alpha}^{\mathrm{WP}}(r_2)Y_{l_\alpha m_\alpha}(\hat{\boldsymbol{r}}_2).\end{aligned} \tag{22}$$

From the normalization condition

$$\left\langle\psi_\alpha^{\mathrm{WP}}\middle|\psi_\alpha^{\mathrm{WP}}\right\rangle=1, \tag{23}$$

one finds that

$$\nu_{n_\alpha l_\alpha}=\left[2\left(\left\langle R_{n_\alpha l_\alpha}^{\mathrm{WP}}\middle|R_{n_\alpha l_\alpha}^{\mathrm{WP}}\right\rangle+\delta_{l_\alpha 0}\delta_{m_\alpha 0}\left\langle R_{n_\alpha l_\alpha}^{\mathrm{WP}}\middle|R_{1s}^{\mathrm{He}^+}\right\rangle\right)\right]^{-1/2}. \tag{24}$$

For atomic hydrogen, these normalization coefficients were directly related to the width of the ith bin [12]. In addition, condition (20) ensures the orthogonality of the wave-packet pseudostates:

$$\left\langle\psi_\alpha^{\mathrm{WP}}\middle|\psi_{\alpha'}^{\mathrm{WP}}\right\rangle=\delta_{\alpha'\alpha}. \tag{25}$$

N_c wave-packet pseudostates representing the $[0,E_{\max}]$ region of the active electron continuum, together with N_b bound states, form a practically complete set of pseudostates for a particular angular momentum l, provided N_c and N_b are sufficiently large. Including other angular momenta, the total number of channels becomes $N=\sum_{l=0}^{l_{\max}}(2l+1)(N_b-l+N_c)$, where $l_{\max}$ is the maximum allowed angular momentum. The number of negative- and positive-energy states is increased until adequate convergence is achieved in the predicted cross sections that we are interested in.

B. Scattering amplitudes

The full scattering amplitude can be calculated from the scattering wave function Ψ_i^+ according to [38,39]

$$T_{fi}(\boldsymbol{q}_f,\boldsymbol{q}_i)=\langle\Phi_f^-|\overleftarrow{H}-E|\Psi_i^+\rangle, \tag{26}$$

where $\boldsymbol{q}_f$ and $\boldsymbol{q}_i$ are the momenta of the scattered and incident projectile, respectively, Φ_f^- is the asymptotic wave function describing the final state, and the arrow over the four-body Hamiltonian operator H indicates the direction of its action. As discussed in Ref. [12], scattering amplitudes for the transitions into bound states of the target are directly defined by the transition amplitudes $T_{fi}^N(\boldsymbol{q}_f,\boldsymbol{q}_i)$, whereas the scattering amplitude for ionization of the active electron with momentum $\boldsymbol{\kappa}$ contains the overlap between the two-electron wave packet ψ_f^{WP} and the active electron's continuum functions φ_f defined in Eq. (15). Accordingly, the ionization amplitude is written as

$$\begin{aligned}T_{\boldsymbol{\kappa}i}(\boldsymbol{q}_f,\boldsymbol{q}_i)=&\left\langle\varphi_f\middle|\psi_f^{\mathrm{WP}}\right\rangle T_{fi}^N(\boldsymbol{q}_f,\boldsymbol{q}_i)\\=&\sum_{l=0}^{l_{\max}}\sum_{m=-l}^{l}\frac{(-i)^l e^{i\sigma_l}Y_{lm}(\hat{\boldsymbol{\kappa}})T_{nlmi}^N(\boldsymbol{q}_f,\boldsymbol{q}_i)}{2\pi\kappa\sqrt{w_n}},\end{aligned} \tag{27}$$

where the index n corresponds to the bin with width w_n and $\kappa=\kappa_n=\sqrt{2\mathcal{E}_n}$. Consequently, both excitation and ionization amplitudes are obtained upon calculation of the transition matrix elements $T_{fi}^N(\boldsymbol{q}_f,\boldsymbol{q}_i)$, which are related to the impact-parameter space transition probability amplitudes through [40]

$$\begin{aligned}T_{fi}^N(\boldsymbol{q}_f,\boldsymbol{q}_i)=&\frac{1}{2\pi}\int d\boldsymbol{b}e^{i\boldsymbol{p}_\perp\boldsymbol{b}}[a_f(\infty,\boldsymbol{b})-\delta_{fi}]\\=&e^{im(\varphi_f+\pi/2)}\int_0^\infty dbb[\tilde{a}_f(\infty,b)-\delta_{fi}]J_m(p_\perp b),\end{aligned} \tag{28}$$

where $\boldsymbol{p}=\boldsymbol{q}_i-\boldsymbol{q}_f$ and $\tilde{a}_f(t,b)=e^{im\phi_b}a_f(t,\boldsymbol{b})$. The required impact-parameter space transition probability amplitudes themselves are obtained by solving the system of differential equations (8) using standard Runge-Kutta routines. Depending on the type of the pseudostates utilized, the matrix elements in Eq. (8) are calculated using the strategy that works best for that particular case. For Laguerre pseudostates the calculation strategy for the matrix elements is described in Ref. [36]. With the proposed wave-packet pseudostates, they are calculated using the expression

$$\begin{aligned}\langle\psi_\alpha|V|\psi_\beta\rangle=&\,2X[\varphi_\alpha,\varphi_\beta]+2\left\langle\phi_{1s}^{\mathrm{He}^+}\middle|\varphi_\beta\right\rangle X\left[\varphi_\alpha,\phi_{1s}^{\mathrm{He}^+}\right]\\&+2\left\langle\varphi_\alpha\middle|\phi_{1s}^{\mathrm{He}^+}\right\rangle X\left[\phi_{1s}^{\mathrm{He}^+},\varphi_\beta\right]\\&+2\left\langle\varphi_\alpha\middle|\varphi_\beta\right\rangle X\left[\phi_{1s}^{\mathrm{He}^+},\phi_{1s}^{\mathrm{He}^+}\right],\end{aligned} \tag{29}$$

where

$$X[f,g]=\int d\boldsymbol{r}\,f(\boldsymbol{r})\left(-\frac{1}{R}+\frac{1}{|\boldsymbol{R}-\boldsymbol{r}|}\right)g(\boldsymbol{r}) \tag{30}$$

is the one-electron transition matrix element similar to that emerging in the formulation of antiproton-hydrogen collisions. Details of $X[f,g]$ are given in Ref. [41].

Once the scattering amplitudes have been obtained, various differential and integrated cross sections can be calculated as described in Ref. [12].

III. DETAILS OF CALCULATIONS

In this section we provide some details of our antiproton-helium calculations. As mentioned earlier, the present calculations are based on the frozen-core approximation to the helium target. Consequently, any of the target states considered can be characterized with a set of only three quantum numbers

$\{n,l,m\}$ representing the active electron. The strategy used for convergence studies of the final results, therefore, can be the same as that used for antiproton-hydrogen collisions [12], where the target states were also described by the same set of quantum numbers.

Several parameters associated with the target and the projectile need to be investigated to establish the convergence of the predictions. Parameters characterizing the active electron of the target, such as the maximum allowed orbital quantum number $l_{\max}$, the number of bound (negative-energy) eigenstates $N_b - l$, the maximum energy $E_{\max}$ of the active electron continuum covered by wave-packet bins, and the number of bins within this interval N_c, define the overall target structure. Each of these parameters is systematically increased while fixing the others at sufficiently large values. This procedure is continued until the parameter-dependent variation of the results is reduced to a level of less than 1% . For antiproton-helium collisions at intermediate and high energies, this was achieved with $l_{\max} = 7$, $N_b = 10 - l$, $E_{\max} = 400$ eV, and $N_c = 30$.

With the above parameters, the total number of target states in the present calculations was $N = \sum_{l=0}^{l_{\max}}(N_b + N_c - l)(2l + 1) = 2112$ at all antiproton energies considered. This number also defines the size of the system of coupled differential equations (8). Another parameter that determines the accuracy of the target structure calculations is the number of quadrature points for integration within each bin. It was chosen depending on the width of the bin. Typically, at least 40 points were used for the small bins, and the number of points was increased for larger bins as required.

The target-structure parameters, which produced converged results for antiproton impact single ionization of helium, also yield converged results for the proton impact at 1-MeV incident energy considered in this paper. At this impact energy, electron-capture channels associated with proton projectiles are negligible compared to the direct ionization channel. Hence the single-center close-coupling approach developed here is adequate.

Apart from establishing convergence of the final results with respect to the target-structure parameters, we also validated our code by switching off the coupling between the discretized channels. We obtained excellent agreement with the first Born results calculated in the full treatment. Unlike in the case of proton or antiproton impact ionization of hydrogen, for the helium target there is no closed analytical expression for the ionization amplitude. However, it is possible to numerically calculate the wave version of the first Born amplitude in the helium frozen-core approximation by using the partial-wave expansion method. This method of calculating ionization amplitude requires the direct use of the active-electron continuum function instead of the wave packets. In this case one can compare the results obtained using the continuum functions and the wave packets for each partial-wave term individually.

Finally, we also obtained convergent results with respect to the parameters associated with the projectile. The set of coupled differential equations (8) was solved by varying the z component ($z \equiv vt$) of the projectile position from -200 to $+200$ a.u. at all energies. The upper limit for the impact parameter $b_{\max}$ was proportionally increased from 10 a.u. at 1 keV to 40 a.u. at 1 MeV. At all considered energies the radial grid required for the calculations of the matrix elements was extended up to 500 a.u..

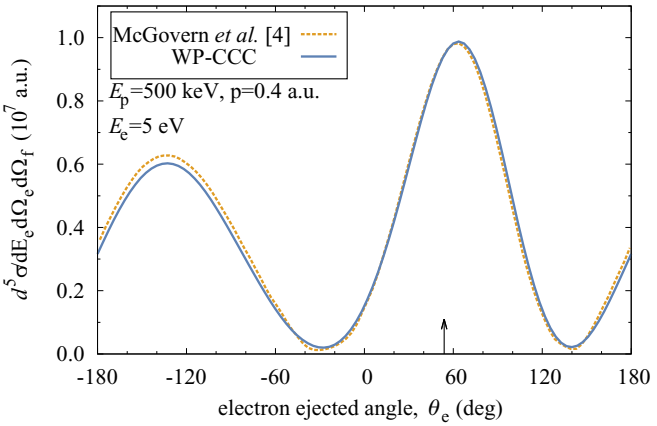

FIG. 1. Fully differential cross section in the collision plane for antiproton impact ionization of helium in its ground state for a projectile energy E_p, momentum transfer p, and energy of the ejected electron E_e. The results of the semiclassical CP approach of McGovern *et al.* [4] are also shown. The arrow indicates the direction of the momentum transfer.

To ensure consistency of our calculations, we always pay particular attention to obtaining the same total ionization cross section by either summing over the partial cross sections for excitation of the positive-energy states or by integrating the fully (fivefold) differential cross section

$$\frac{d^5\sigma(\boldsymbol{q}_f,\boldsymbol{q}_i,\boldsymbol{\kappa})}{dE\,d\Omega_e\,d\Omega_f} = \mu^2\frac{q_f\kappa}{q_i}|T_{\kappa i}(\boldsymbol{q}_f,\boldsymbol{q}_i)|^2 \qquad (31)$$

over all variables. The fully differential cross section describes a scattering event when the electron is ejected into the solid angle $d\Omega_e$ around the direction $\Omega_e = (\theta_e,\phi_e)$ with the energy between E and $E + dE$, while the projectile is scattered into the solid angle $d\Omega_f$ around the direction $\Omega_f = (\theta_f,\phi_f)$.

IV. RESULTS AND DISCUSSION

In this section we present our wave-packet based CCC (WP-CCC) results for antiproton-helium fully and partially differential ionization cross sections, as well as the total ionization cross section. The collision geometries and projectile energies are chosen in a way that allows for the most comprehensive comparison with our quantum-mechanical CCC results published in Ref. [36] and predictions from other semiclassical theories [4,5]. Lastly, we show in-plane and out-of-plane triply differential single-ionization cross sections for 1-MeV proton-helium collisions, which were obtained using the present single-center convergent close-coupling approach, and compare them with recent experimental data [31].

A. Single ionization of He by antiprotons

Figure 1 exhibits our results for the fully differential cross section in the collision plane for 1-MeV antiproton helium collisions. The present WP-CCC results are compared with the coupled-pseudostate (CP) calculations of McGovern *et al.* [4].

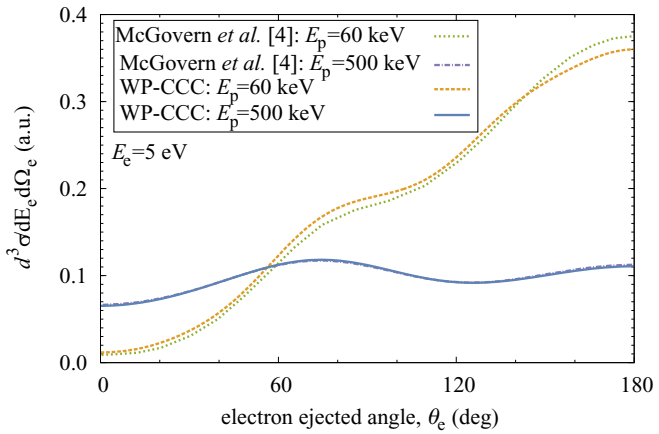

FIG. 2. The triply differential cross section $d^3\sigma/dE_e d\Omega_e$ for antiproton impact ionization of helium at 60 and 500 keV for the ejected-electron energy of 5 eV. The present WP-CCC results are compared with those of the coupled pseudostates approach of McGovern *et al.* [4].

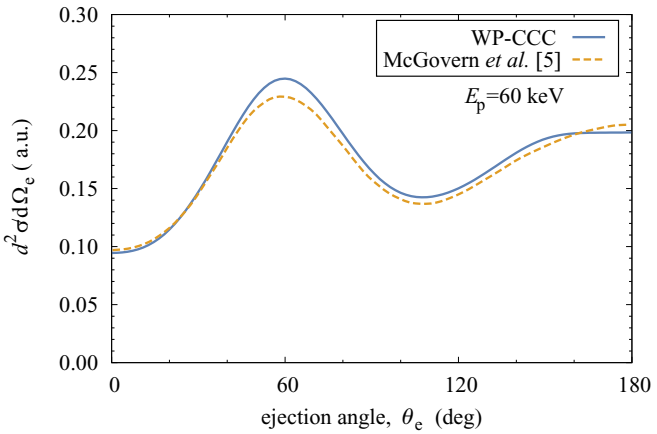

FIG. 3. The doubly differential cross section $d^2\sigma/d\Omega_e$ for antiproton impact single ionization of helium at 60 keV. Results of the coupled pseudostates approach of McGovern *et al.* [5] are also presented.

Here the direction of the scattered antiprotons is fixed and given by the value of the momentum transfer, $p = 0.4$ a.u., while the electron-ejection angle θ_e runs from -180 to 180° relative to the direction of the incident antiproton. Since the coplanar geometry is considered, the azimuthal coordinates of the ejected electron ϕ_e and the antiproton ϕ_f are set to zero. The arrow indicates the direction of the momentum transfer $\boldsymbol{p}$. The ejected-electron energy is fixed at 5 eV. We note that the flexibility of the presently developed WP basis in distributing the positive-energy states arbitrarily allows us to have a state with energy 5 eV for all l. This helps to improve the accuracy of the calculations.

As seen from the figure, for every indicated antiproton energy and momentum transfer the WP-CCC and the CP calculations of McGovern *et al.* [4] are in excellent agreement. Both theories predict the binary and recoil peaks at the same electron-ejection angle, which qualitatively describes the phenomenon of suppressed electron ejection along the direction of the scattered antiprotons (essentially near the forward direction). Due to the repulsive Coulomb force between the antiproton and the electron, the binary peak is shifted to the right from the momentum-transfer direction.

The triply differential (in energy and two-dimensional solid angle of the ejected electron) cross sections (TDCSs) [42], $d^3\sigma/dE_e d\Omega_e$, are presented in Fig. 2 for the ejected-electron energy of $E_e = 5$ eV and various energies of the incident antiproton as a function of the electron-ejection angle θ_e. The results of the coupled-pseudostate approach of McGovern *et al.* [4] are also shown for comparison. Since this TDCS is formed by integrating the FDCS over the solid angle of the projectile, the results displayed in Fig. 1 retain some features of the corresponding FDCS shown in Fig. 1. As expected, electron emission is suppressed at small ejection angles when the projectile energy is low and relatively flat at the higher energy. The features seen around 80° and at 180° are results from integration over the binary and recoil peaks of the FDCS, respectively. The small difference between the WP-CCC and CP results of McGovern *et al.* [4] could be due to the absence of a Laguerre pseudostate exactly at 5 eV in the latter calculations.

Figure 3 displays our results for the doubly differential cross section in the ejection angle of the electron, $d^2\sigma/d\Omega_e$, in comparison with the calculations of McGovern *et al.* [4]. The presently calculated cross section has a small maximum at zero ejection angle, a more pronounced maximum around 60°, and a minimum around 110°. The relatively large cross section in the backward direction indicates the propensity for the electron to be ejected in the opposite direction to the antiproton. The agreement between the present WP-CCC results and the semiclassical approaches of McGovern *et al.* [5] is generally good.

Carrying out kinematically complete experiments is a complicated task due to the difficulties related with the production of a stable high-intensity antiproton beam. However, the recent developments of recoil-ion and ejected-electron momentum spectroscopy make accurate measurements of differential cross sections in the momenta of these particles possible. In fact, the recoil ion carries as much information on the three-body ionization dynamics as the projectile and the ejected electron. Such a pioneering experiment [14] on antiproton impact ionization of He was reported at 945 keV, where the singly differential cross section was measured as a function of the longitudinal recoil-ion and the ejected-electron momenta.

These quantities can be obtained from the triply differential ionization cross section $d^3\sigma(q_f, q_i, \boldsymbol{\kappa})/dE d\Omega_e$ if we impose the following dynamic constraints required by energy and momentum conservation:

$$p_{r\parallel} = p_\parallel - \kappa_\parallel = \frac{\epsilon_f - \epsilon_0}{v} - \kappa\cos\theta_e, \tag{32}$$

where $p_{r\parallel}$ and $\kappa_\parallel$ are, respectively, the longitudinal momenta for the recoil ion and the ionized electron, while $p_\parallel$ is the longitudinal projectile momentum transfer. With this we can write

$$\frac{d\sigma}{d\kappa_\parallel} = \int_{\kappa_\parallel^2/2}^{\infty} \frac{1}{\kappa}\frac{d^2\sigma}{dE d\Omega_e} dE, \tag{33}$$

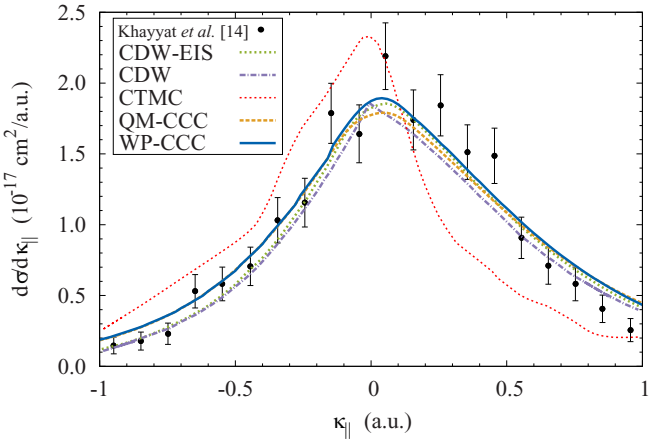

FIG. 4. Ejected-electron longitudinal momentum distribution for single ionization of helium by 945-keV antiproton impact. The experimental data, CDW, and CTMC calculations are due to Khayyat *et al.* [14]. The CDW-EIS and QM-CCC calculations are due to Fainstein and Rodriguez [13] and Abdurakhmanov *et al.* [36].

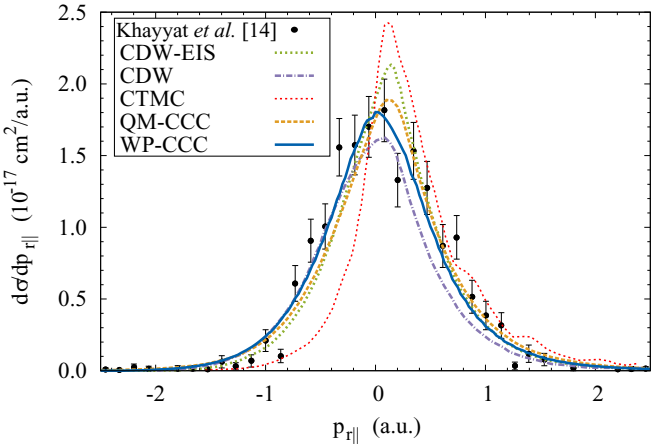

FIG. 5. Recoil-ion longitudinal momentum distribution for single ionization of helium by 945-keV antiproton impact. The experimental data, CDW, and CTMC calculations are due to Khayyat *et al.* [14], and the CDW-EIS calculations are due to Fainstein and Rodriguez [13]. The frozen-core QM-CCC calculations are from [36].

and

$$\frac{d\sigma}{dp_{r\parallel}} = \int_{\epsilon^-}^{\epsilon^+} \frac{1}{\kappa} \frac{d^2\sigma}{dE d\Omega_e} dE. \tag{34}$$

The integration limits of Eq. (34) can be obtained from Eq. (32) or the relationship

$$\kappa^{\pm} = v\cos\theta_e \pm \sqrt{v^2\cos^2\theta_e + 2(p_{r\parallel}v - |\epsilon_0|)} \tag{35}$$

using $\epsilon^{\pm} = (\kappa^{\pm})^2/2$.

Figure 4 shows the ejected-electron longitudinal momentum distribution in single ionization of helium by antiproton impact at 945 keV. We compare our FC results with the experimental data of Khayyat *et al.* [14] and predictions from continuum distorted-wave (CDW), classical trajectory Monte Carlo (CTMC), continuum distorted-wave eikonal initial state (CDW-EIS) and QM-CCC calculations. Apart from the CTMC calculations, there is reasonably good agreement between the various theories and experiment.

The corresponding recoil-ion longitudinal momentum distribution is given in Fig. 5. Only the CTMC approach clearly fails to reproduce the experimental data. The CDW results show a systematic discrepancy at positive momentum values. Similar measurements, but at lower impact energies, would be helpful in testing the theoretical approaches to fully differential ionization by antiproton impact.

Figure 6 shows the total cross section for antiproton impact single ionization of helium for incident energies ranging from 1 keV to 1 MeV. The latest experiment was carried out at CERN [43], where data were obtained starting from antiproton impact energies as low as 3.42 keV. These measurements exhibit a rather slow falloff of the cross section with the decreasing impact energy. We see that the highest two energy points of this dataset agree reasonably well with the earlier experiment by Hvelplund *et al.* [44], which itself is in overall agreement with the first experiment reported by Andersen *et al.* [45].

The lines represent various theoretical calculations based on the frozen-core approximation of the helium target [4,15,19,36]. All of these calculations start off by diagonalizing the helium Hamiltonian in a suitable two-electron basis with the assumption that the inner electron is always in the ground state. The only difference is that different representations of the radial part of the target active electron wave function are used: wave-packet bin pseudostates in the present approach, Slater-type orbitals by Lee *et al.* [19], Sturmian functions by Igarashi *et al.* [15], and Laguerre functions by McGovern *et al.* [4] and Abdurakhmanov *et al.* [36]. The calculation of Abdurakhmanov *et al.* [36] also differs from the others by the fact that the approach is fully quantum mechanical. All presented calculations are in quite good agreement with each other and experiment above 100 keV. However, below 100 keV there is some

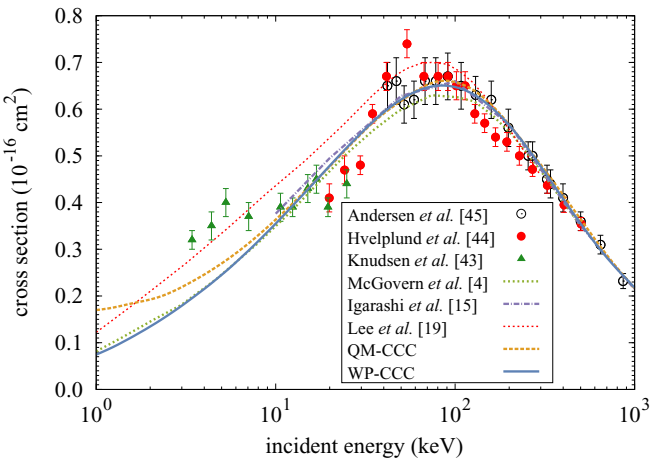

FIG. 6. Total single-ionization cross section for antiproton-helium scattering. The present calculations (WP-CCC) are compared with experimental data by Knudsen *et al.* [43], Andersen *et al.* [45] and Hvelplund *et al.* [44], QM-CCC results [36], and various semiclassical calculations by McGovern *et al.* [4], Igarashi *et al.* [15], and Lee *et al.* [19].

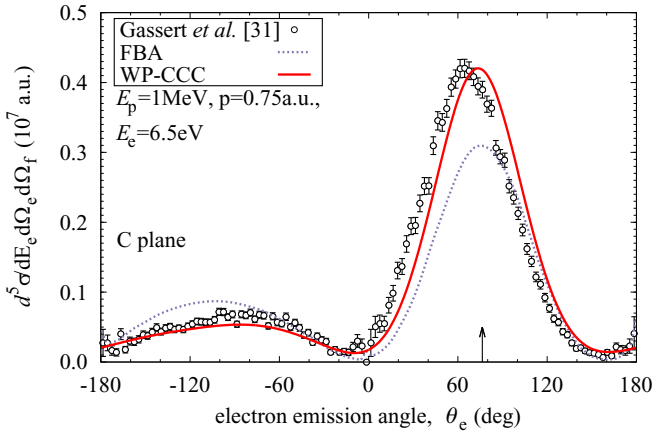

FIG. 7. Fully differential cross sections for single ionization of helium by 1-MeV protons in the collision plane. The electron emission energy is $E_e = 6.5$ eV, and the total momentum transfer $p = 0.75$ a.u. The present calculations (WP-CCC) are compared with the experimental data and FBA calculations by Gassert *et al.* [31]. The arrow indicates the direction of the momentum transfer.

variation and also disagreement with the experiment. This may indicate that a more accurate multicore treatment of the helium target is required to reproduce the low-energy behavior of the total ionization cross section. The semiclassical straight-line trajectory approximation is expected to slowly deteriorate with reducing energy, therefore around 1 keV QM-CCC is more reliable as it is fully quantum mechanical and does not use a straight-line trajectory. Interestingly, using a more accurate description of the helium target, beyond the frozen-core approximation, will likely result in a reduction of the predicted cross sections, at least at high energies [23,36]. Assuming the experimental data are normalized correctly, an improvement in the theoretical description may thus lead to a slight deterioration of the agreement between theory and experiment. This issue will be addressed in our future studies.

B. Single ionization of He by 1-MeV protons

A recent experiment by Gassert *et al.* [31] provided data on the fully differential cross sections for single ionization of helium by 1-MeV protons in the collision plane and several other planar geometries. Since this is in the high-energy regime, the present single-center close-coupling approach can be applied with confidence to calculate the cross sections for the measured differential ionization data. Here the electron capture channels associated with proton impact are expected to be several orders of magnitude less important than the direct ionization channels and, consequently, can be neglected.

Figure 7 compares our results for the FDCS in the collision (C) plane with the experimental data and the first Born approximation calculations of Gassert *et al.* [31,46]. For this scattering regime, where the ejected-electron energy is 6.5 eV and the scattering angle of the protons is given by the momentum transfer of $p = 0.75$ a.u., we see good agreement with experiment at all electron emission angles considered here. Furthermore, in comparison with the FBA results, the present calculations show better agreement with experiment at the electron emission angles in the region from -180 to 80° and around 180°. The experimental data peak at about $\theta_e = 61.5^\circ$, while our results peak at 73.5°. This is a slight improvement from the first Born calculations that peak at 76.5°. The WP-CCC results are fully convergent (within the frozen-core approximation). Therefore, we believe that the

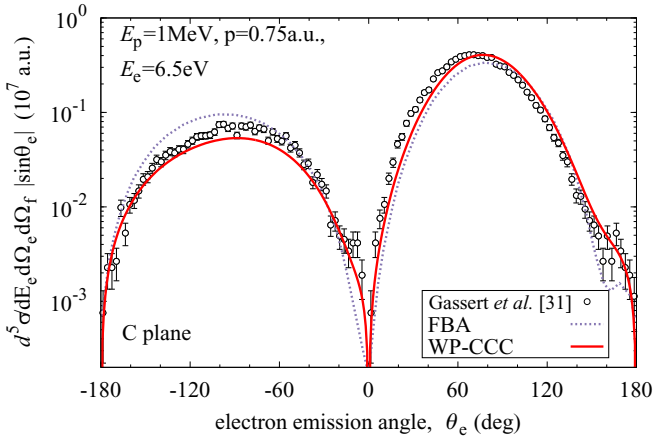

FIG. 8. Same as in Fig. 7 but multiplied by $|\sin\theta_e|$.

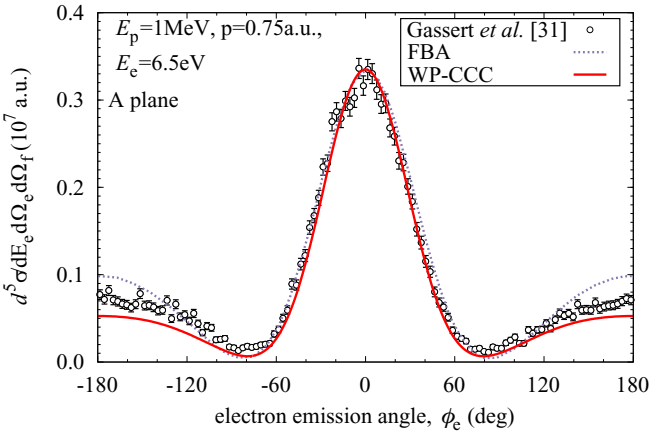

FIG. 9. Same as in Fig. 7 but for emission into the azimuthal plane ($\theta_e = 90^\circ$) given as a function of the azimuthal emission angle ϕ_e.

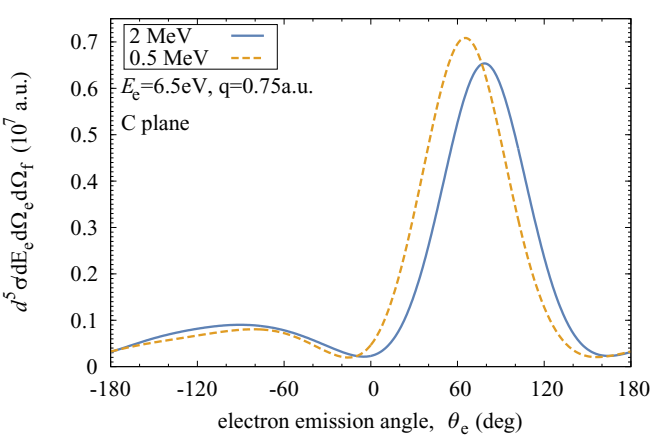

FIG. 10. Same as in Fig. 7 but for 0.5- and 2-MeV protons.

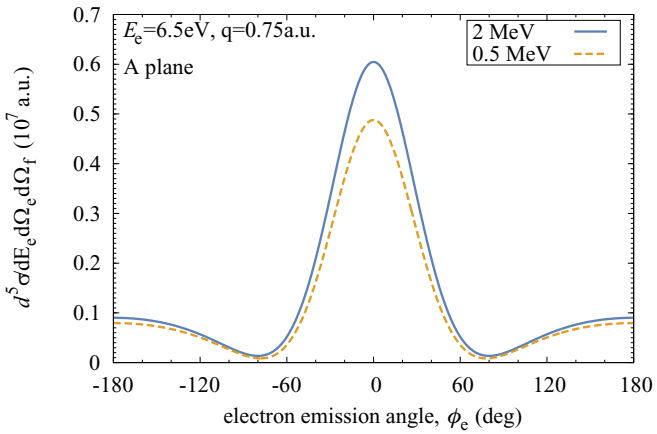

FIG. 11. Same as in Fig. 9 but for 0.5- and 2-MeV protons.

remaining discrepancy in the peak angle could be due to the frozen-core approximation used. A multicore approach may lead to a better agreement with the experiment. At the same time, we have to mention that the experimental angular resolution is reported to be $\pm 10^\circ$ [31]. So, the aforementioned discrepancy is very close to the experimental uncertainty.

The same FDCSs but multiplied by $|\sin\theta_e|$ (as presented in Ref. [31]) are shown in Fig. 8, which highlights the vicinity of the node separating the binary and the recoil peak. Note that the experimental peak shifts to $\theta_e = 67.5^\circ$. The maximum of the WP-CCC results shifts to 77°. However, there is nothing physical in the shift and it is purely due to the extra $|\sin\theta_e|$ factor in the FDCS.

Figure 9 shows the same comparison for the azimuthal (A) plane ($\theta_e = 90^\circ$). Here we also see good agreement with experiment at almost all electron emission angles considered. At backward electron emission angles, the present results lie slightly below the measured data, whereas the previous FBA results were slightly higher. Note that the WP-CCC results are fully symmetric around $\phi_e = 0^\circ$.

Figures 10 and 11 show our predictions for the FDCS in the collision and azimuthal planes for 0.5- and 2-MeV protons, in anticipation of experimental data [47] at these impact energies.

V. CONCLUSIONS AND OUTLOOK

The problem of antiproton scattering from helium has been considered within the framework of the recently developed wave-packet based target continuum-discretization approach [12]. The electron-electron correlation of the target was taken into account in the frozen-core approximation. Two-electron wave functions describing the target were built from a linear combination of products of one-electron functions representing the core ion of He^+ and the active electron. While the He^+ core was described by its ground-state wave function, the basis of active-electron functions was generated from numerically calculated discrete negative-energy state wave functions and continuum wave packets. The wave packets are the integrals of the radial continuum wave function over the regions of the bins discretizing the continuum. The energies of the continuum wave packets were chosen so that they aligned for different orbital angular momenta.

The above approach is ideal for detailed differential ionization studies. The density of the continuum discretization can be as high as necessary. The generated orthonormal basis of two-electron wave functions was used in the target-based one-center expansion of the total scattering wave function. This converts the semiclassical three-body Schrödinger equation into a set of coupled-channel differential equations, which need to be solved for a range of impact parameters. A comprehensive set of results, from integrated to fully differential cross sections for antiproton impact single ionization of helium in the energy range from 1 keV to 1 MeV, was generated.

Furthermore, we applied our wave-packet single-center convergent close-coupling approach to study fully differential single ionization of helium by 1-MeV proton impact. This was done by changing the charge of the projectile in the code for antiproton-helium scattering. Our calculations are in very good agreement with recent experimental measurements [31] for all experimentally considered geometries. Predictions for 0.5- and 2-MeV protons are also given, in anticipation of further measurements.

The development of a multicore treatment of the helium target based on the wave-packet target continuum-discretization approach is planned for the near future. This will not only improve the accuracy of the predicted cross sections for single-electron processes but also enable the calculation of cross sections for two-electron processes. Extension of the two-center CCC method [48] to the proton-helium system is currently underway.

ACKNOWLEDGMENTS

This work was supported by the Australian Research Council. We are grateful for access to the Australian National Computing Infrastructure Facility and the Pawsey Supercomputing Centre in Western Australia. We also acknowledge partial support from the NSF under Grants No. PHY-1415656 (A.S.K.) and No. PHY-1403245 (K.B.). We thank Markus Schöffler for providing the experimental data of Ref. [31] in a tabulated form.

[1] S. Yu, B. Logan, J. Barnard, F. Bieniosek, R. Briggs, R. Cohen, J. Coleman, R. Davidson, A. Friedman, E. Gilson, L. Grisham, D. Grote, E. Henestroza, I. Kaganovich, M. K. Covo, R. Kishek, J. Kwan, E. Lee, M. Leitner, S. Lund, A. Molvik, C. Olson, H. Qin, P. Roy, A. Sefkow, P. Seidl, E. Startsev, J.-L. Vay, W. Waldron, and D. Welch, Nucl. Fusion **47**, 721 (2007).

[2] D. Belkic, J. Math. Chem. **47**, 1366 (2010).

[3] M. H. Martir, A. L. Ford, J. F. Reading, and R. L. Becker, J. Phys. B **15**, 1729 (1982).

[4] M. McGovern, D. Assafrão, J. R. Mohallem, C. T. Whelan, and H. R. J. Walters, Phys. Rev. A **79**, 042707 (2009).

[5] M. McGovern, D. Assafrão, J. R. Mohallem, C. T. Whelan, and H. R. J. Walters, Phys. Rev. A **81**, 032708 (2010).

[6] K. A. Hall, J. F. Reading, and A. L. Ford, J. Phys. B **29**, 6123 (1996).

[7] A. Igarashi, S. Nakazaki, and A. Ohsaki, Phys. Rev. A **61**, 062712 (2000).

[8] S. Sahoo, S. C. Mukherjee, and H. R. J. Walters, J. Phys. B **37**, 3227 (2004).

[9] J. Azuma, N. Toshima, K. Hino, and A. Igarashi, Phys. Rev. A **64**, 062704 (2001).

[10] B. Pons, Phys. Rev. Lett. **84**, 4569 (2000).

[11] N. Toshima, Phys. Rev. A **64**, 024701 (2001).

[12] I. B. Abdurakhmanov, A. S. Kadyrov, and I. Bray, Phys. Rev. A **94**, 022703 (2016).

[13] P. D. Fainstein and V. D. Rodriguez, J. Phys. B **33**, 4637 (2000).

[14] K. Khayyat, T. Weber, R. Dörner, M. Achler, V. Mergel, L. Spielberger, O. Jagutzki, U. Meyer, J. Ullrich, R. Moshammer, W. Schmitt, H. Knudsen, U. Mikkelsen, P. Aggerholm, E. Uggerhoej, S. P. Moeller, V. D. Rodriguez, S. F. C. O'Rourke, R. E. Olson, P. D. Fainstein, J. H. McGuire, and H. Schmidt-Böcking, J. Phys. B **32**, L73 (1999).

[15] A. Igarashi, A. Ohsaki, and S. Nakazaki, Phys. Rev. A **62**, 052722 (2000).

[16] G. Schiwietz, U. Wille, R. D. Muiño, P. D. Fainstein, and P. L. Grande, J. Phys. B **29**, 307 (1996).

[17] L. A. Wehrman, A. L. Ford, and J. F. Reading, J. Phys. B **29**, 5831 (1996).

[18] S. Sahoo, S. Mukherjee, and H. Walters, Nucl. Instrum. Methods B **233**, 318 (2005).

[19] T. G. Lee, H. C. Tseng, and C. D. Lin, Phys. Rev. A **61**, 062713 (2000).

[20] F. Martin and A. Salin, Phys. Rev. A **54**, 3990 (1996).

[21] M. S. Pindzola, T. G. Lee, and J. Colgan, J. Phys. B **44**, 205204 (2011).

[22] M. Foster, J. Colgan, and M. S. Pindzola, Phys. Rev. Lett. **100**, 033201 (2008).

[23] X. Guan and K. Bartschat, Phys. Rev. Lett. **103**, 213201 (2009).

[24] A. Igarashi, A. Ohsaki, and S. Nakazaki, Phys. Rev. A **64**, 042717 (2001).

[25] I. B. Abdurakhmanov, A. S. Kadyrov, I. Bray, and A. T. Stelbovics, J. Phys. B **44**, 075204 (2011).

[26] I. B. Abdurakhmanov, A. S. Kadyrov, I. Bray, and A. T. Stelbovics, J. Phys. B **44**, 165203 (2011).

[27] S. Borbély, J. Feist, K. Tőkési, S. Nagele, L. Nagy, and J. Burgdörfer, Phys. Rev. A **90**, 052706 (2014).

[28] M. Baxter and T. Kirchner, Phys. Rev. A **87**, 062507 (2013).

[29] M. Baxter and T. Kirchner, Phys. Rev. A **93**, 012502 (2016).

[30] I. F. Barna, N. Grün, and W. Scheid, Eur. Phys. J. D **25**, 239 (2003).

[31] H. Gassert, O. Chuluunbaatar, M. Waitz, F. Trinter, H.-K. Kim, T. Bauer, A. Laucke, C. Müller, J. Voigtsberger, M. Weller, J. Rist, M. Pitzer, S. Zeller, T. Jahnke, L. P. H. Schmidt, J. B. Williams, S. A. Zaytsev, A. A. Bulychev, K. A. Kouzakov, H. Schmidt-Böcking, R. Dörner, Y. V. Popov, and M. S. Schöffler, Phys. Rev. Lett. **116**, 073201 (2016).

[32] M. Schulz, R. Moshammer, D. Fischer, H. Kollmus, D. H. Madison, S. Jones, and J. Ullrich, Nature (London) **422**, 48 (2003).

[33] I. B. Abdurakhmanov, A. S. Kadyrov, D. V. Fursa, S. K. Avazbaev, J. J. Bailey, and I. Bray, Phys. Rev. A **91**, 022712 (2015).

[34] I. B. Abdurakhmanov, A. S. Kadyrov, D. V. Fursa, S. K. Avazbaev, and I. Bray, Phys. Rev. A **89**, 042706 (2014).

[35] B. H. Bransden and M. R. C. McDowell, *Charge Exchange and the Theory of Ion-Atom Collisions* (Clarendon, Oxford, 1992).

[36] I. B. Abdurakhmanov, A. S. Kadyrov, D. V. Fursa, I. Bray, and A. T. Stelbovics, Phys. Rev. A **84**, 062708 (2011).

[37] C. E. Moore, *Atomic Energy Levels as Derived from Analyses of Optical Spectra*, Circ. No. 467 Vol. 1 (Natl. Bur. Stand. U.S., U.S. GPO, Washington, D.C., 1949).

[38] A. S. Kadyrov, I. Bray, A. M. Mukhamedzhanov, and A. T. Stelbovics, Phys. Rev. Lett. **101**, 230405 (2008).

[39] A. S. Kadyrov, I. Bray, A. M. Mukhamedzhanov, and A. T. Stelbovics, Ann. Phys. **324**, 1516 (2009).

[40] Since we work with the full interaction potential, the transition probability amplitudes include the heavy-particle interaction; see Eq. (6).

[41] I. B. Abdurakhmanov, A. S. Kadyrov, I. Bray, and A. T. Stelbovics, J. Phys. Conference Series **388**, 082015 (2012).

[42] Usually, this triply differential cross section is called a doubly differential cross section; however, since in this paper we consider more than coplanar geometries we have to move away from this convention.

[43] H. Knudsen, H.-P. E. Kristiansen, H. D. Thomsen, U. I. Uggerhøj, T. Ichioka, S. P. Møller, C. A. Hunniford, R. W. McCullough, M. Charlton, N. Kuroda, Y. Nagata, H. A. Torii, Y. Yamazaki, H. Imao, H. H. Andersen, and K. Tökesi, Phys. Rev. Lett. **101**, 043201 (2008).

[44] P. Hvelplund, H. Knudsen, U. Mikkelsen, E. Morenzoni, S. P. Moller, E. Uggerhoj, and T. Worm, J. Phys. B **27**, 925 (1994).

[45] L. H. Andersen, P. Hvelplund, H. Knudsen, S. P. Moller, J. O. P. Pedersen, S. Tang-Petersen, E. Uggerhoj, K. Elsener, and E. Morenzoni, Phys. Rev. A **41**, 6536 (1990).

[46] The experimental results for the FDCS have been obtained from the raw data presented in Fig. 2(c) of Ref. [31] by dividing the latter by $|\sin\theta_e|$.

[47] M. S. Schöffler, 2017 (private communication).

[48] S. K. Avazbaev, A. S. Kadyrov, I. B. Abdurakhmanov, D. V. Fursa, and I. Bray, Phys. Rev. A **93**, 022710 (2016).